Springer

KSME

Journal of Mechanical Science and Technology 00 (2016) 0000~0000

www.springerlink.com/content/1738-494x
submitted manuscript under review

Wall Shear Stress and Velocity Distributions in Different Types of Stenotic Bifurcations

K. Kanokjaruvijit[1*], T. Donprai-on[1], N. Phanthura[1], P. Noidet[1] and J. Siripokharattana[2]

[1]*Department of Mechanical Engineering, Naresuan University, Pitsanulok, 65000, Thailand*
[2]*Department of Mechanical and Automotive Engineering Technology, Faculty of Engineering and Technology, King Mongkut's University of Technology North Bangkok, Rayong, 21120, Thailand*

(Manuscript Received 000 0, 2009; Revised 000 0, 2009; Accepted 000 0, 2009) -please leave blank

Abstract

Blood flow following Carreau-Yasuda viscosity model at steady-state through various categories of stenotic arterial bifurcations based on Movahed [1] was investigated by using finite element method. Reynolds number was fixed at 233. Results are reported in terms of wall shear stress (WSS) and velocity distributions. The maximum peaks of WSS was found at the minimum flow area, where high velocities were present. Symmetric stenotic sites gives rather symmetric WSS distribution and symmetric velocity profile, whereas on asymmetric sites, the skewness depends upon the presence of the stenotic site as it introduces curvature. Volumetric flow rate ratios at various locations were introduced to indicate the crucial conditions. In addition, levels of stenosis between 30-60% based on flow area were considered. The 60% level gave significant higher WSS peak and the lowest WSS at the location behind the stenosis for the symmetric case. For the asymmetric case, the 50 and 60% levels show the lowest WSS values at the end of the stenotic site.

Keywords: Bifurcation; Carreau-Yasuda; Finite element; Movahed classification; Wall shear stress

1. Introduction

Atherosclerotic lesions have been known associated to the vessel wall shear stress variation. The tentative sites of atherosclerotic participation are those locations, where the blood flow changes its direction such as curvature, junctions and bifurcations. Hence, the detailed information of wall shear stress is important especially to cardiologists. Bifurcations have been brought to numerous researchers' interests, and there have been significant classifications of coronary bifurcations such as Sanborn, Lefevre, Safian, Duke, Medina and Movahed [1]. While the first four classifications were used during the bare metal stent time, the last two are appropriate and adaptive to the current intervention technique for bifurcations using drug-eluting stents [1].

Advancement in computer software and hardware development has made a non-intrusive method such as the numerical method with non-Newtonian viscosity models become more possible and effective. Hence, the computational fluid dynamic method has been adopted as a tool to evaluate vascular physiological quantities such as wall shear stress instead of conducting experiments. Johnston et al. [2] tested 5 different viscosity models via wall shear stress patterns with 4 different right coronary arteries at steady state in order to find the appropriate viscosity models that can imitate blood flow. The models were Newtonian, Carreau-Yasuda, Walburn-Schneck, Power law and Casson models. They stated that no single model can universally represent blood. Nonetheless, the fact that blood behaves as a Newtonian fluid at shear rate less than 100 s^{-1} showed that the power law and the Walburn-Schneck models did not show this behavior. The Carreau-Yasuda model was suggested as it fit experimental data quite well. The results were also confirmed by Gijsen et al. [3] and presented the flattened axial velocity profiles due to its shear thinning behavior. Additionally, Husain et al.[4] investigated 4 viscosity models such as power law, Casson, Carreau and generalized power law through a stenosed artery. The pressure drop values obtained from these models were compared to those from the Newtonian model. They found that all non-Newtonian models except the power law model gave higher pressure drop than the Newtonian.

Bifurcation is prone to atherosclerotic plaque due to the changes in flow directions and curvature causing flow separation and back flow, thus fluctuating the wall shear stress values away from their normal range of 0.5-1.5 Pa

† This paper was recommended for publication in revised form by Associate Editor 000 000-please leave blank.
*Corresponding author. Tel.: +66 55964210, Fax.: +66 55964000
E-mail address: koonlaya@gmail.com, koonlayak@nu.ac.th

in an artery [5]. Therefore, there have been various researches conducted on blood flow through different shapes of bifurcations. For instance, a carotid arterial bifurcation has been interested by many researchers as it contains curvature and non-planar branching, which affects the flow features. Zhao et al. [6] and Long et al. [7] used a reconstructed model from magnetic resonance images of a carotid arterial bifurcation of a healthy man to numerically study the Newtonian blood flow. Gijsen et al. [3] also studied blood flow through *in vitro* experiments and a finite element method of an arterial carotid at steady state using both Non-Newtonian and Newtonian fluids. Their results were in agreement that the secondary flow or Dean vortex was found at the curvature from the transition from the common carotid and the internal carotid. Increase and decrease of the vessel cross-sectional areas decelerated and accelerated the flow, respectively, which affected the axial velocity profiles and the wall shear stress significantly.

In addition, flow through coronary bifurcations also catch researchers' interests as they are significantly related to cardiovascular diseases. Due to their complex geometry, the effects of curvature on the flow and the WSS patterns were focused. Chen and Lu [8-9] investigated a geometric bifurcation with one non-planar curved branch. Weydahl and Moore [10] used a geometrically- curved bifurcation model. The effect of curvature of a left anterior descending coronary artery realistic model and its first diagonal branch was studied by Prosi et al.[11]. Another interesting research work was conducted by Gijsen et al. [12] on a blood flow through a 90-degree curved tube using the Carreau-Yasuda model. Skewness of the peak of velocity distribution occurred toward the inner bend. In addition, Dean vortices took place resulting in a shift of the peak value toward the outer wall.

A straight vessel with stenosis has been investigated by several researchers. Flow and WSS patterns significantly depended on stenosis severity according to Husain [4,13]. The maximum WSS occurred just before the stenotic throat, and further downstream the WSS values became undisturbed [4]. Wang and Berndolf [13] examined steady Newtonian and non-Newtonian Carreau-Yasuda blood flow through cubic-spline shaped stenotic straight tubes with 30 and 70% stenosis. Longer recirculation after the stenosis was found in the Newtonian case due to lower shear rate causing high viscosity in the non-Newtonian case. Shuib et al.[14] tested 2D Newtonian laminar and turbulence blood flow through a stenotic vessel at different Reynolds numbers. The blood flow through a 90^{o}-step and a smooth sudden expanded tubes were compared by Hyun et al.[15], and found that the step expansion was less prone to atherosclerosis.

Few researches were carried out on the blood flow through 3D stenotic bifurcations of any classifications. Zarandi et al.[16] presented blood flow conditions through stenotic coronary arterial bifurcations in the context of Medina classification. Three cases of stenotics in the main branch proximal and/or the main branch distal and the side branch were carried out. The stenotic lesions were made axi-symmetric for 50 and 75% stenosis levels. Wall shear stress patterns were presented along with the flow distributions in order to conclude which stenosis type was more prone to atherosclerosis progression.

Most of researches on blood flow through stenosis have been carried out in a straight tube and through axi-symmetric lesions without being in the context of any classification. Therefore, this current research was aimed to numerically study the blood flow through different types of stenotic arterial bifurcations according to Movahed classification by using a non-Newtonian viscosity model of Carreau-Yasuda at various stenosis levels. The finite element method was employed under steady-state condition at a fixed Reynolds number of 233, while the effect of pulsatile flow is planned for our following paper. Patterns of values of wall shear stress are presented as well as axial velocity profiles.

2. Methodology

2.1 Assumptions and problem scope

The blood flow through an arterial bifurcation at steady-state and laminar flow was assumed at diastole corresponding to Reynolds number of 233 [3]. The blood behaved in accordance with Carreau-Yasuda viscosity model. Shown in Fig.1, the bifurcation vessel consists of mother vessel having diameter of 4.0 mm, and was then divided to 2 branches namely primary and secondary daughter vessels having 3.2 mm and 2.8 mm diameters, respectively. All vessel wall were assumed rigid and followed no-slip condition. Furthermore, the stenosis level in terms of percentage is calculated based on the minimum flow area of the stenotic site compared to the flow area of the vessel before the stenotic site. The flow left the bifurcation at the exit of each daughter vessel toward zero gauge pressure. This was done in order to imitate an *in vitro* experimental setup.

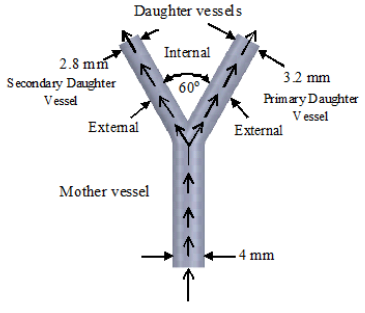

Fig.1. Bifurcation with normal condition and boundary conditions.

2.2 Computational Domain

Stenotic bifurcations were categorized based on the stenosis of arterial bifurcation categorization of Movahed [1] as illustrated in Fig.2. Note that Movahed [1] classified the stenotic bifurcation into 7 cases, namely 1m, 1s, S, L, 2, V and T, but in this study L, 2 and V types were combined to one case due to its similarity. Hence, here there are 5 types called 1m, 1s, S, L-2-V and T instead. Type 1m in Fig.2(a) contains stenosiss on both internal and external sides of the primary daughter vessel whereas type 1s shown in Fig.2(b) contains stenosiss on both sides of its secondary daughter vessel. Fig.2(c) presents type S which the stenosiss occur at the external side of the primary daughter vessel and the internal side of the secondary daughter vessel. The presence of stenosiss for types L-2-V and T in Figs.2(d) and (e) are similar, except for the fact that type T has an obtuse angle of 110° between the daughter vessels while type L-2-V and the rest have acute angles of 60°, and appear on both internal and external sides of both daughter vessels. Note that the stenosis on the external side of the primary daughter vessel for each related case also covers some part of the mother vessel. The stenosis percentage was calculated as minimum flow area over the diameter of the daughter vessel, where the stenosis was present.

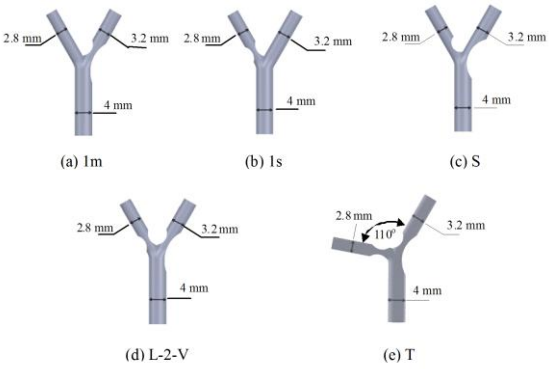

Fig.2. Category of stenosiss in bifurcation based on the categorization of Movahed [1]. Note that the maximum stenotic areas cover 50% of flow area in each vessel.

2.3 Governing equations

As the steady-state and laminar 3D flow was assumed throughout the study, the governing equations are as follows

Continuity Equation:

$$\nabla \cdot \vec{u} = 0 \tag{1}$$

Momentum Equations :

$$\rho\left(\frac{\partial \vec{u}}{\partial t} + \vec{u} \cdot \nabla \vec{u}\right) = -\nabla P + \mu \nabla^2 \vec{u} \tag{2}$$

where $\vec{u}$ denotes velocity of the blood, ρ is the blood density and equal to 1,050 kg/m^3, P is the fluid pressure and μ represents the dynamic viscosity of the blood, which behaves according to the Carreau-Yasuda model [17] and the values of parameters and constants were obtained from Gijsen et al.[3] as follows

$$\mu = \mu_\infty + (\mu_0 - \mu_\infty)[1 + (\lambda \nabla \vec{u})^a]^{\frac{n-1}{a}} \tag{3}$$

where μ_∞ is the viscosity of the blood when the infinite shear applies = 2.2×10^{-3} Pa-s, μ_0 is the viscosity of the blood when the minimum shear applies = 22×10^{-3} Pa-s, λ is the characteristic time constant = 0.110 s, n = 0.392 and a = 0.644. Note that the properties of all fluids used throughout this study are at 37°C.

Once the velocities were solved, the wall shear rate, $\dot{\gamma}$, was then calculated from

$$\dot{\gamma} = \frac{du_i}{dx_j} \tag{4}$$

Finally, the wall shear stress, WSS, was computed from the product of the wall shear rate and the Carreau-Yasuda viscosity as follows

$$WSS = \mu \cdot \dot{\gamma} \tag{5}$$

The results are reported in terms of the wall shear stress values and the flow fields or velocity profiles in the next section.

2.4 Numerical Method

The finite element method was used to discretized the hemodynamic problem via a commercial software COMSOL in order to approximate the dependent variables u, v, w and P. Once the computational domain was set, unstructured 3D meshes were generated using free meshing algorithm. For the Navier-Stokes equation system, second order Lagrange elements model the velocity components, and linear elements model the pressure. A second-order Lagrange or quadratic element contains node points at the corners and side midpoints of all mesh, and a linear element contains node points at the corners only. For each node point p_i, there is a degree of freedom $U_i = u(p_i)$ and a basis function ϕ_i. The major constraint of the basis function ϕ_i is then a polynomial of degree 2 in the local coordinates. Hence, ϕ_i = 1 at node i and ϕ_i = 0 at other nodes. Therefore, the basis functions are then continuous and $u = \sum U_i \phi_i$.

The governing equations are nonlinear partial differential equation system. Since our problems are at steady state, the stationary solver breaks down the nonlinear system into several linear equations. Then, the UMFPACK algorithm, which is a direct solver for asymmetric systems using the asymmetric-pattern multifrontal method and direct LU factorization of a sparse matrix, performs the solving process once the boundary conditions are applied in order to obtain matrices of u, v, w and P with tolerance of 10^{-6}.

2.5 Mesh density dependence check

Unstructured meshes were generated throughout the vessels using the Delaunay algorithm with the boundaries partitioned into triangular elements. Prior to beginning the investigation on the flow through stenotic bifurcations, mesh density dependence check needed to be carried out for the normal bifurcation using Carreau-Yasuda viscosity model. Three mesh densities were tested: 11.85

meshes/mm^3 (Model A), 46.81 meshes/mm^3 (Model B) and 147.43 meshes/mm^3 (Model C) using adaptive mesh refinement.

Two cross sections measured 10 mm away from the entry, called X-X', and at the bifurcation region, Y-Y', where the flow was divided to two daughter vessels as illustrated in Fig.3. The computed results were shown in terms of wall shear stress values in Figs.4 and 5 for the cross sections X-X' and Y-Y', respectively.

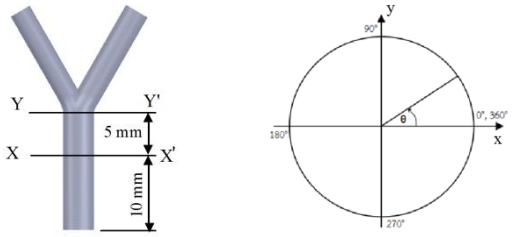

(a) Locations of cross sections (b) Locations in terms of degrees along a circle peripheral

Fig.3. Locations of cross sections taken for mesh density dependence check.

Fig.4 shows the wall shear stress values at the cross section in the mother vessel, which is similar to the circular tube. All mesh densities gave harmonized results. The average values of WSS are 1.4256, 1.4361 and 1.4897 Pa for Models A, B and C, respectively. The wall shear stress values near the end of the mother vessel or the beginning of bifurcated daughter vessels present the fluctuating pattern for all three mesh densities in Fig.5. This was because the flow prepared to be divided and the flow symmetry was being destroyed. Local comparison suggested that the maximum difference around 20.63% occurs at around 250^o between the WSS values of Models B and C. This was also due to that fact that the denominator was low.

According to the study by Holzbecher and Si [18], the adaptive mesh refinements led to more accurate solutions judging from less errors. This happened especially to quadratic elements. However, finer meshes consume the computational memory and time, and sometimes lead to divergence of the solutions. Therefore, in this study, a mesh density of 46.81 elements/mm^3 was chosen as a compromise between accuracy and convergence. Note that Intel Core i3 CPU with 4 GB RAM Computer was used in the entire investigation.

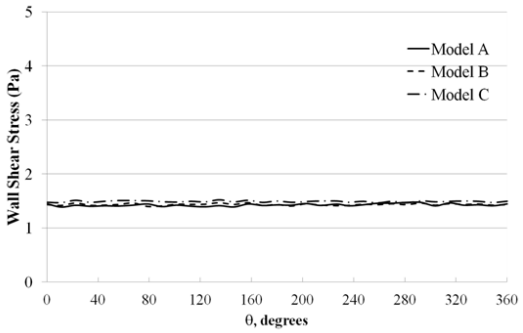

Fig.4. Comparison of wall shear stress of the cross section at 10 mm away from the mother vessel entry (X-X') for different mesh densities

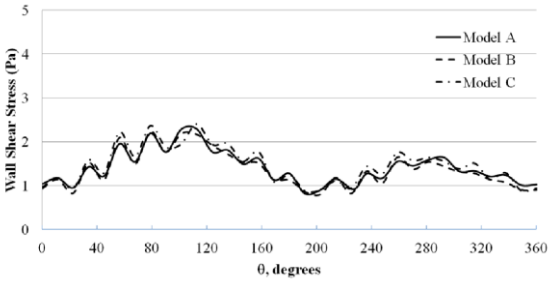

Fig.5. Comparison of wall shear stress of the cross section at the bifurcation region (Y-Y') for different mesh densities.

3. Results and Discussion

3.1 Validation

Fig.6 shows the comparison of dimensionless velocities (V/V_{max}) of the present study of cross sections at z = 10, 15 mm measured from the entrance of the mother vessel and at the beginning of the bifurcation, where the flow started to divide, to those obtained from literature, for the bifurcation without stenosis. Good agreement was found between the dimensionless velocities measured 10 mm away from the main entrance and the results of Boyd et al.[19], who used the Lattice method. The profile is flat in the middle of the vessel. At 15 mm away from the entrance, half of the profile became collapse to the results of Gijsen et al.[7], who also used the Carreau-Yasuda viscosity model, while the other half showed the difference. This was thought due to the fact that Gijsen et al.[7] examined the blood flow through a carotid artery, whose daughter vessels are significantly different in diameters. This effect was also observed in the profile at the beginning of the bifurcation, where the flow from the mother vessel was getting split.

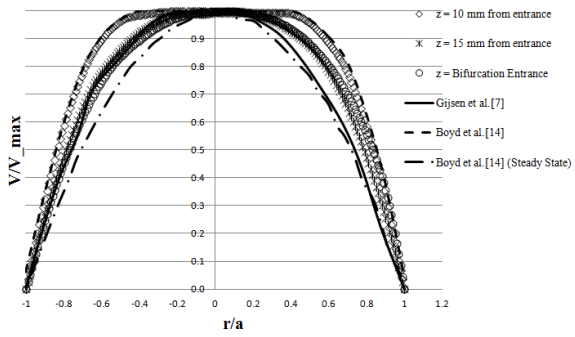

Fig.6. Comparison of dimensionless velocities at different cross sections along the mother vessel of bifurcation to literature.

3.2 Stenotic bifurcation classification

The WSS distributions and the axial velocity profiles for each bifurcation are discussed here. This section starts with the WSS and the flow distributions of normal Y and T bifurcations. Then, the following subsection deals with the various types of stenotic bifurcations. Note that since local hemodynamics helps understand the cause of lesion generation especially after the stenotic sites, each case of stenosis is worth being discussed individually in this section. Finally, the levels of stenosis will be discussed in the last subsection.

3.2.1 Normal Y and T Bifurcations

WSS along the mother vessel and both daughter vessels are reported for both Y and T bifurcations without stenosis as illustrated in Figs.7 and 8. The similarity of the trend was found along the mother vessel until the flow arrived the bifurcation section, where the flow was to be divided to the daughter vessels. For the Y-bifurcation, after the bifurcation area the WSS in the primary daughter vessel is by overall higher than that in the secondary one whereas the opposite results were found for the T-bifurcation. Fig.9 presents the comparison of the WSS of the secondary daughter vessels of both types of bifurcation. The WSS in the mother vessel of the Y-bifurcation is higher, while in the secondary daughter vessel the T-bifurcation gave higher value.

Flow fields in Fig.10(a) suggests that for the Y-Bifurcation the daughter vessels were separated by the angle of 60°, and the angle between the mother vessel and each daughter vessel was equal to 30°. However, since the primary vessel was larger, more flow was diverted towards it than the secondary one. Thus, the WSS was higher in the primary vessel (Fig.7). For the T-bifurcation, of which the daughter vessels were separated by the angle of 110°, Fig.10(b) shows that the flow in the secondary daughter vessel was strongly skewed towards the inner wall compared to that in the primary vessel. This could be the explanation for the higher value of WSS in Fig.8. As for the explanation for Fig.9, the blood turned sharply in the secondary daughter vessel for the T-bifurcation compared to that for the Y-bifurcation. This could cause the higher shear.

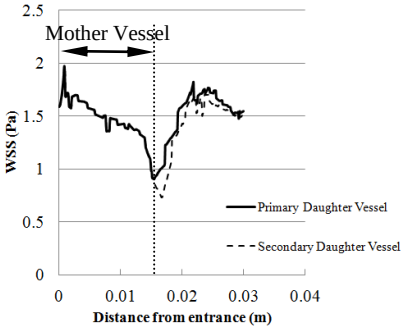

Fig.7. WSS along a normal Y-bifurcation with 60° between the daughter vessels (without stenosis).

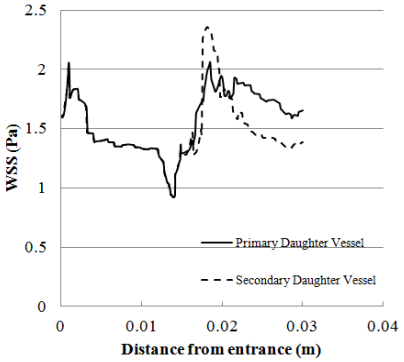

Fig.8. WSS along a normal T-bifurcation with 110° between the daughter vessels (without stenosis).

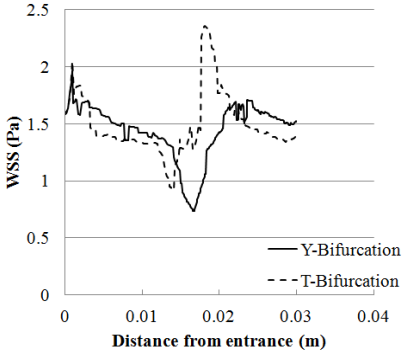

Fig.9. Comparison of WSS along secondary daughter vessels of normal Y and T-bifurcations.

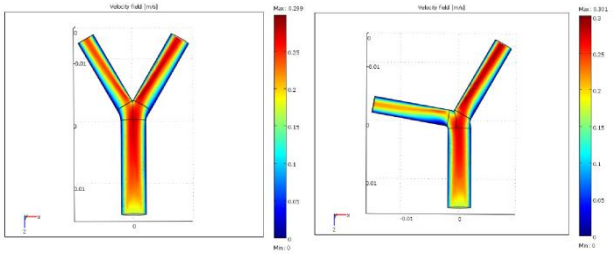

(a) Y-Bifurcation (b) T-Bifurcation

Fig.10. Overall flow fields in the entire bifurcations.

3.2.2 *Stenotic bifurcations*

(a) Type 1m

Figs.11(a) and (b) show WSS patterns along front wall and stenotic sites, respectively, for the stenotic bifurcation type 1m. Along the front walls, the values of WSS from the entrance in the mother vessel through the beginning of the primary daughter vessel are likely in the normal range (0.5-1.5 Pa [4]), even where the stenosis on the outer side was present. However, the curvature of such stenosis insignificantly affected the flow as shown in the flow field in Fig.11(c). This also shows along the stenotic sites in Fig.11(b) on the outer wall. Then, the maximum peak of WSS was found at the minimum flow area, where the stenotic sites were present on both sides of the primary daughter vessel. This represents the high velocity vicinity in the flow field of Fig.11(c), where the flow looked like being squeezed through a narrow channel. Finally, once the blood flow was expanded, the WSS values became lower than 1 in both Fig.11(a) and (b). This occurred in the low velocity region after the stenotic sites in Fig.11(c).

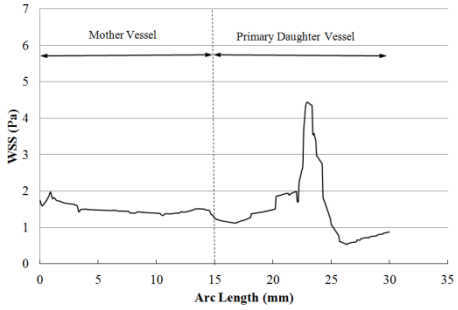

(a) WSS pattern along front side

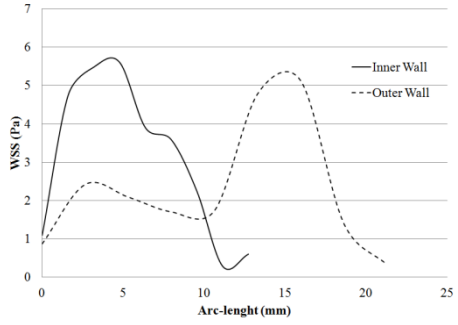

(b) WSS pattern at stenotic sites

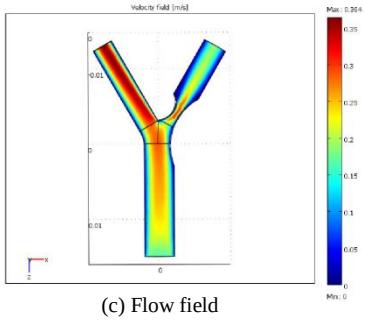

(c) Flow field

Fig.11. WSS and flow distributions for the stenosis type 1m.

(b) Type 1s

Fig.12 shows the WSS patterns and flow field for the stenosis type 1s, which has stenotic sites with same curvature on each side of the secondary daughter vessel. The trend of WSS distribution on the front side in Fig.12(a) was not as severe as that of type 1m. Most of the WSS values were approximately in the normal range with the peak value of around 2.6 Pa, slightly higher than the higher limit of the normal range. Considering Fig.12(b), which illustrates the WSS pattern along the stenotic sites of both inner and outer wall, there are two peaks of the WSS on the inner wall and one nearly symmetric peak on the outer wall. The flow field illustrated in Fig.12(c) shows that the first peak the blood flow is skewed toward the inner wall. For the second peak, which occurred at the narrowest flow area, the flow is seemingly squeezed then expanded, which correspond to the rapid drop of WSS. Note that the flow velocity profiles are likely symmetric when the flow was passing the stenotic sites.

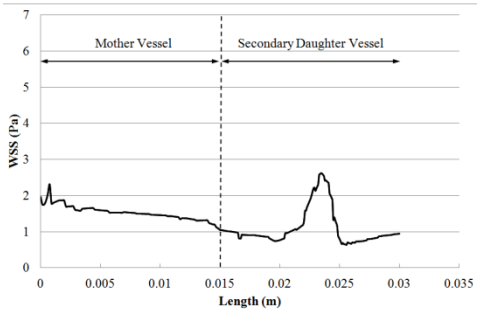

(a) Front view through secondary daughter vessel

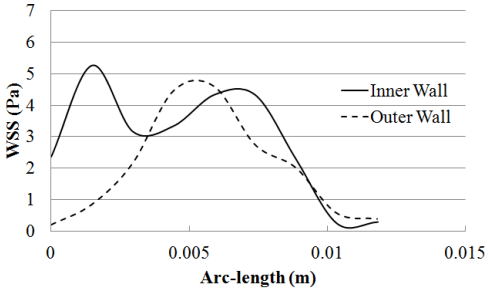

(b) At stenotic sites

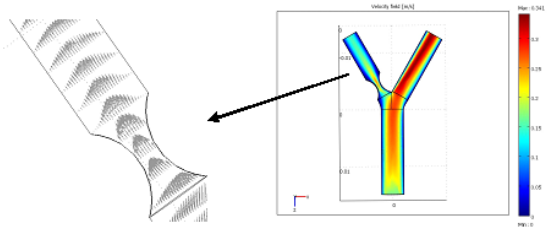

(c) Flow field

Fig.12. WSS and flow distributions for the stenosis type 1s.

(c) Type S

The stenotic sites for type S are located at 2 sites: on the

mother vessel to the outer side of the primary daughter vessel and on the inner side of the secondary daughter vessel with smaller curvature. Fig.13(a) presents the WSS distribution along the front wall. The curvature of larger stenotic site did not affect the blood flow much in the mother vessel as the WSS values are still in the normal range. Once the flow reached the bifurcation region, the curvature started playing an important role, and caused smaller flow passage (see Fig.13(c)). The on-site WSS, then, rapidly increased to the peak of 6.8 Pa for the primary daughter vessel as shown in Fig.13(b). In the secondary daughter vessel, the convex site started at apex, where the flow from the mother vessel impacted on, and caused the highest value of WSS of 11.5 Pa at the beginning of the site. Then, the WSS decreased to 3 Pa after the apex, and increased to another peak of 9 Pa at the narrowest flow passage. At the end of the convex sites of both daughter vessels, the WSS dropped rapidly. Fig.13(c) shows that the flow was deflected by the convex site toward the other side of each vessel. In addition, skewness of the flow toward the inner wall of each daughter vessel occurred in a normal bifurcation was likely to disappear on the convex sites in type S. This presents in parabola velocity profiles in the narrow flow passages in Fig.13(c). At the end of the stenosis, the flow separation occurred on the outer wall of the primary daughter vessel and on the inner wall of the secondary daughter vessel.

(d) Type L-2-V

The stenotic sites of type L-2-V are located on both inner and outer walls of both daughter vessels. Both convex sites on the inner and outer walls of the secondary daughter vessel were designed to be identical. However, the primary daughter vessel contained asymmetric convex sites as shown in Fig.2(d) with a larger curvature on the outer wall. Fig.14(a) presents WSS distribution on the front view from the entrance of the mother vessel to the exits of both daughter vessels. Similar shapes were found with different peak values of 6.3 and 5 Pa for the primary and the secondary daughter vessels, respectively. The WSS distribution at the stenotic sites of the primary daughter vessel are illustrated in Fig.14(b). The convex surface on the mother vessel slightly affected the blood flow by increasing the WSS value to approximately 2.5 Pa. However, the peaks values of both branches were similar at 7.3 Pa. Then, the WSS was reduced to below 1 Pa at the ends of the stenotic sites. This could be explained by the appearance of flow separation in Fig.14(d). After the stenosiss, the blood flow became more parabolic without skewness towards the inner wall.

Considering the symmetry of the stenotic sites in the secondary daughter vessel in Fig.14(c), both maximum peaks are approximately the same at 7 Pa. Notwithstanding that, the shapes at the inner and outer walls are different. At the beginning of the inner wall, the WSS increases rapidly, because some amount of the flow from the mother vessel was deflected by the convex site on the mother vessel wall, and also the stenotic site on the inner wall started right at the apex, where the flow from the mother vessel impacted, see Fig.14(d). Then, the plateau shape of WSS occurred along the convex surface of the inner wall. However, the WSS of the outer wall gradually increased to the peak value near the narrowest flow passage. Once, the flow had passed the stenotic sites, the WSS decreased to near zero due to the flow separation. Then, the velocity profiles in Fig.14(d) became more symmetric through the exit without a sign of skewness.

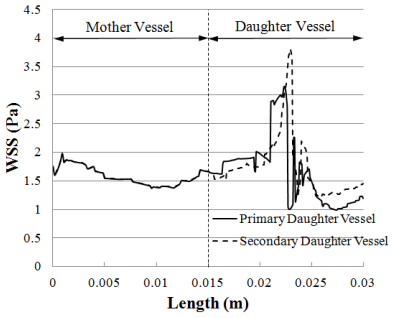

(a) Front view through each secondary daughter vessel.

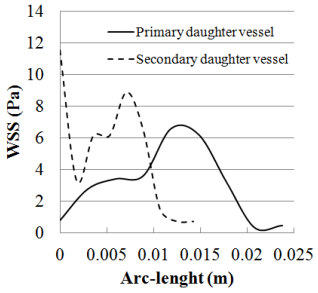

(b) At stenotic sites

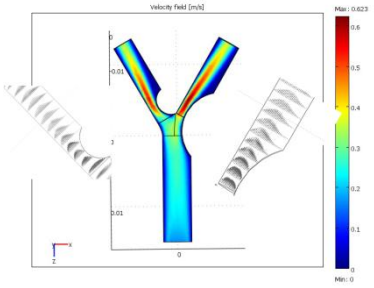

(c) Flow field

Fig.13. WSS and velocity distributions for stenosis type S.

(e) Type T

The stenotic sites of type T bifurcation are similar to those of type L-2-V in the previous section, except for the bifurcation angle between the primary and the secondary daughter vessels, of which type T is 110 degrees. The angle between the axis and the secondary daughter vessel here became 80 degrees, and that between the axis. Fig.15(a) represents the WSS distribution along the front side of the entire bifurcation. At the end of the mother

vessel and the beginning of each daughter vessel, the WSS became greater than 2 Pa, which is greater than that of type L-2-V. The WSS on the secondary daughter vessel dropped to 1.75 Pa and increased to the peak of 5.5 Pa. Contrarily, the WSS on the primary daughter vessel rather gradually increased until the flow passage became narrower, the WSS then raised to the maximum value of 4.3 Pa. Finally, the WSS of both daughter vessels decreased to approximately 0.5 Pa, and increased again to a normal range along the expanded passage.

The WSS distribution along the stenotic sites of the primary daughter vessel are presented in Fig.15(b). Starting with 2.5 Pa for the inner wall, the maximum value was 9.5 Pa, and rapidly decreased to near zero at the end of the site. The pattern of the WSS of the site on the outer wall is similar to that of type L-2-V as well as the maximum peak of 7 Pa. Interestingly, the WSS distributions of the secondary daughter vessel shown in Fig.15(c) showed dissimilarity to those of type L-2-V at the beginning of the outer wall stenotic site as it was higher for type T. The maximum peak of the outer wall was approximately 10 Pa, while the inner wall gave the peak of 6.5 Pa. The blood flow from the mother vessel drastically turned to the secondary daughter vessel, and also the convex surface on the mother vessel wall diverted more flow toward the secondary daughter vessel. In addition, the latter influence became more pronounced than type L-2-V as suggested in Fig.15(d). At the end of each site, the WSS value became below 1 Pa. This can be explained by the flow separation found at the end of the convex surface of each wall in Fig.15(d).

(f) Local volumetric flow rate ratio

According to the blood flow analysis through different types of coronary bifurcations in the context of Medina classification of Molavi-Zarandi et al.[16], volumetric flow rate ratio (Q ratio) was employed as a quantitative tool to help indicate the tendency of severity of the flow conditions. Here, the severe cases of stenotic sites occurring on both branches such as types L-2-V and T were selected to present in Table 1. Note that the primary daughter vessels for both cases were equally tilted 30 degrees from the main axis, but the secondary daughter vessel were different. For type L-2-V, it was tilted 30 degrees from the main axis, while for the type T, it was tilted 80 degrees. Q denotes the volumetric flow rate. Subscripts 0, 1, 2, 3, 4, 5, 6 and 7 indicate the locations at the entrance of the main vessel, at the beginning of the stenosis on the main vessel, at the beginning of the stenosis on the primary daughter vessel, at the maximum stenotic site on the primary daughter vessel (the narrowest flow area), after the stenotic site on the primary daughter vessel, at the beginning of the stenotic site on the secondary daughter vessel, at the maximum stenotic site on the secondary daughter vessel (the narrowest flow area) and after the stenotic site on the secondary daughter vessel, respectively.

More crucial conditions were found in the secondary daughter vessel in both cases as the ratios became 20-37%. The significant difference were found in the secondary daughter vessel where type L-2-V gave 73% less at the maximum stenotic site (Q_6) and 27% at the end of the stenosis (Q_7). This helps imply that the restenosis tends to occur more to the L-2-V case than the T case in the secondary daughter vessel. For the primary daughter vessel, the Q ratios (Q_2/Q_0, Q_3/Q_0), however, are reverse between the two types. The crucial condition for type L-2-V occurred at the maximum stenotic site with Q_3/Q_0 = 31.14%, whereas it occurred at the beginning of the stenosis for type T with Q_2/Q_0 = 33.18%.

Table 1 Volumetric ratios at different locations of stenotic sites

Volumetric flow rate ratio	Type L-2-V	Type T
Q_0/Q_0	1	1
Q_1/Q_0	0.6976	0.7055
Q_2/Q_0	0.4768	0.3318
Q_3/Q_0	0.3114	0.4530
Q_4/Q_0	0.4711	0.4881
Q_5/Q_0	0.2061	0.2582
Q_6/Q_0	0.2118	0.3669
Q_7/Q_0	0.2492	0.3171

3.3 Levels of stenosis

Comparison of WSS distribution for stenotic areas of 30, 40, 50 and 60% were investigated in this section. Only types 1m, 1s and T were selected to present the WSS distribution comparisons on the front side as they contained stenotic sites on both inner and outer walls plus their severity compared to other types. Also note that type 1m contains an asymmetric stenosis, while type 1s consists of a symmetric sites. Fig.16 represents the WSS distribution for type 1m. The stenosis level of 60% showed the most severity in WSS distribution. Its peak is 4.5 Pa, and it decreases to 0.5 Pa at the end of the stenotic site, where the expanded flow passage was formed. However, for the other levels, the peaks were in the vicinity of 3 Pa, then the WSS was reduced to normal values of 1-1.5 Pa.

Fig.17 illustrates the WSS distribution at different stenosis levels for type 1s, at which symmetric stenotic sites are located on the secondary daughter vessel. The peak values for each case is around 2.5-3 Pa, but the significant difference occurs at the end of the stenotic site. At levels of 50 and 60% stenosis, the WSS value decreases to 0.5 Pa, and then gradually increases toward 1 Pa. This can be explained by the fact that the blood flow through a narrow passage between stenotic sites abruptly expanded to a normal vessel. Nonetheless, for levels of 30 and 40% stenosis, the stenotic passages were not as narrow, thus, the WSS values after their stenotic sites stayed in the normal range and rather undisturbed.

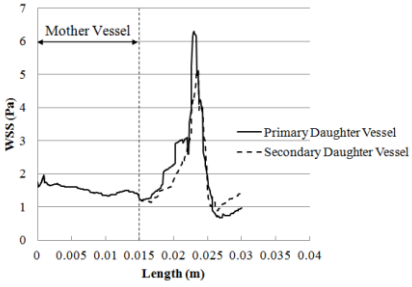

(a) Front view

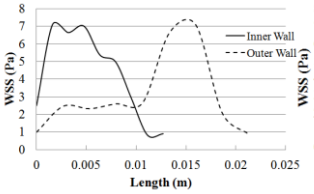

(b) At stenotic sites on primary daughter vessel

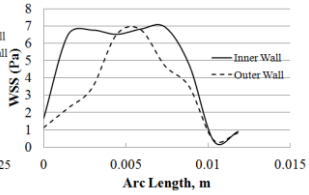

(c) At stenotic sites on secondary daughter vessel

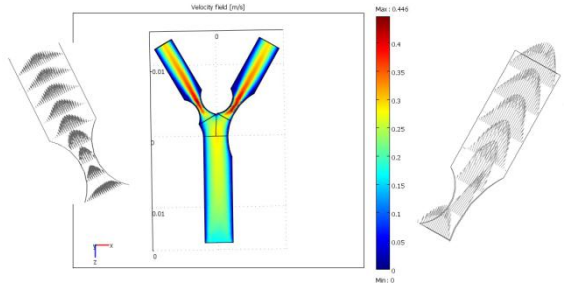

(d) Flow field

Fig.14. WSS distribution for the stenosis type L-2-V.

The WSS patterns of type T stenotic bifurcation are presented in Fig.18 for both primary and secondary daughter vessels. Consider Fig.18(a) for the data of the primary daughter vessel with asymmetric stenotic site, the peak of 30% stenosis was at 3.2 Pa, whereas the rest were between 4.2 and 4.7 Pa. The falloffs at the end of the stenotic sites for 30, 40 and 50% stenosis levels were between 1-1.5 Pa, but 0.5 Pa for 60% stenosis level. Fig.18(b) presents the WSS distributions for the secondary daughter vessel, which was disposed to almost perpendicular to the mother vessel causing all stenosis levels to start with higher WSS values than type 1s, which has similar stenosis geometry. The stenosis level of 50% gave the highest maximum peak of approximately 5.7 Pa followed by the 60% level, which gave 5.5 Pa. After the stenotic site, the WSS values for 30, 40 and 50% levels decreased to an agreeing value of approximately 1.5 Pa. However, the expanded flow passage strongly affected the 60% stenosis case as the WSS drastically decreased to 0.5 Pa prior to increasing back to within the normal range.

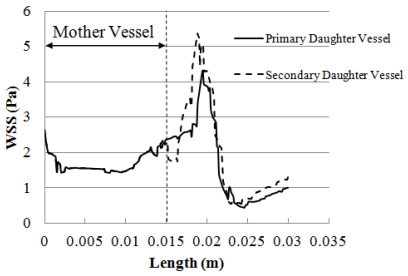

(a) Front view

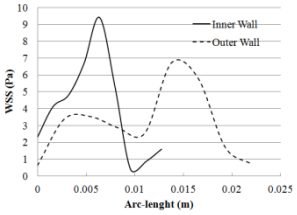

(b) At stenotic sites on primary daughter vessel

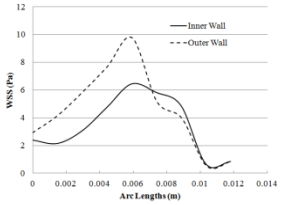

(c) At stenotic sites on secondary daughter vessel

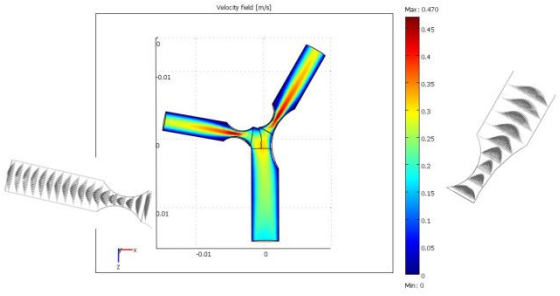

(d) Flow field

Fig.15. WSS distribution for the stenosis type T.

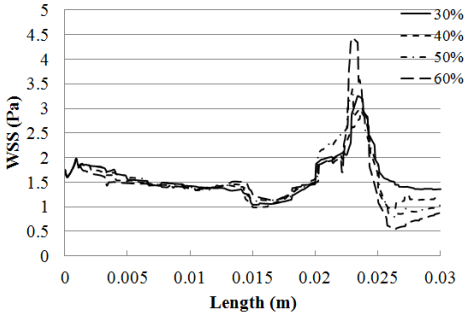

Fig.16. WSS distribution of different levels of stenosis for type 1m.

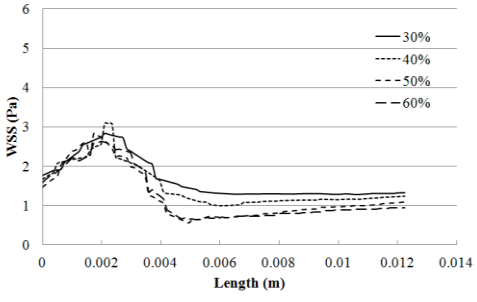

Fig.17. WSS distribution of different levels of stenosis for type 1s.

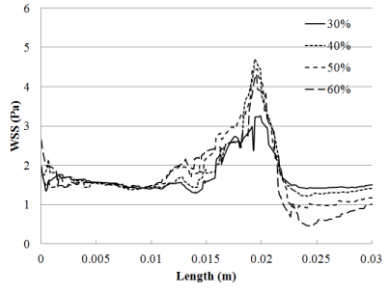

(a) Primary daughter vessel

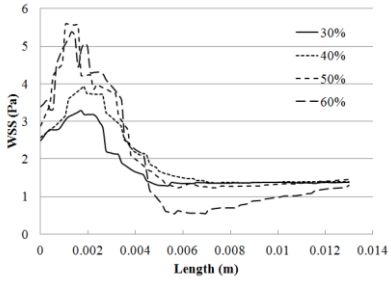

(b) Secondary daughter vessel

Fig.18. WSS distribution of different levels of stenosis for type T.

4. Conclusions

This current study was focused on the patterns of WSS and the flow fields of various types of stenosis in a coronary arterial bifurcation categorized by Movahed [1]. Normal Y- and T-shaped bifurcations were firstly investigated and found the significant difference in the secondary daughter vessels, which were tilted 30 degrees and 80 degrees from the mother vessel, respectively. More severe skewness toward the inner wall was found in the T-type bifurcation resulting in approximately 30% higher in WSS peak compared to that of the Y-type. This was thought due to the nearly sharp turn of the secondary daughter vessel of the T-type.

Five types of stenotic sites were investigated as illustrated in Fig.2: 1m, 1s, S, L-2-V and T. When the stenotic sites were present on both vascular inner and outer walls such as types 1s, L-2-V and T, skewness of the flow field did not play a role. The comparisons the WSS distributions of two-sided stenotic sites such as types 1m and 1s and one-sided sites such as S are considered as follows

- The stenotic sites on the primary daughter vessel of type 1m versus that of type S show no significant difference in local WSS distribution. Flow passage expansion after the stenotic sites for both cases caused flow separation.
- The stenotic sites on the secondary daughter vessel of type 1s versus that of type S gave more obvious different WSS distribution. Two peaks were found in type 1s near the beginning of the stenotic site and at the narrowest passage, while for type S the higher peak was found right at the beginning of the stenotic sites, and another one at the narrowest passage. Stronger flow separation on the inner wall after the stenotic site occurred to type S, whereas the velocity profiles for type 1s were likely symmetric.

Types L-2-V and T were compared due to their same stenosis locations but different angle between the mother vessel and the secondary daughter vessel. The primary daughter vessels of both types showed no significant difference in the WSS values with similar shape. Nonetheless, such difference was found in the secondary daughter vessels of both types, especially on the inner wall possibly owing to more effect of skewness on type L-2-V. The trends of the WSS distributions were similar with higher values from type T. This can be because the flow velocity profiles showed similarity for both stenosis types.

The volumetric flow rate ratio was introduced in order to help indicate the tentative crucial condition according to Zarandi et al.[16]. However, in the current study, different locations along the main and the branch vessels were presented. The crucial conditions tended to occur in the secondary daughter vessel for type L-2-V and in the primary daughter vessel for type T as the volumetric flow rate ratios reduced.

Considering the influence of stenosis level on WSS distribution by varying between 30 and 60% asymmetric stenotic sites on type 1m showed the maximum of WSS peak for the 60% level, while the 50% level gave similar peak value to those of the 30 and 40% levels. The significant differences between each level took place after the stenotic site. Symmetric stenotic site typifying type 1s illustrated similar peaks for all levels, but after the stenotic site, the levels of 50 and 60% gave the lowest WSS and the data almost collapsed. Nevertheless, type T gave the WSS distribution at various stenosis levels different from the other two types. The 50 and 60% stenosis levels gave similar WSS distribution and higher than the 30 and 40% levels, which showed similar distribution in the primary daughter vessel and different distribution in the secondary daughter vessel. This was thought due to the different bifurcating angles from the other cases of bifurcation.

Acknowledgment

This work supported by Research Program supported by ... the contract number ...

Nomenclature

u	: Blood velocity
P	: Blood pressure
Q	: Volumetric flow rate
WSS	: Wall shear stress

$\dot{\gamma}$: Wall shear rate
μ : Blood viscosity
μ_0 : Blood viscosity at minimum shear
μ_∞ : Blood viscosity at infinite shear
ρ : Blood density

References

[1] M. R. Movahed, Coronary artery bifurcation lesion classification, interventional technique and clinical outcome, *Expert Rev Cardiovasc Ther*, 6(2) (2008) 261-274.

[2] B. M. Johnston, P. R. Johnston, S. Corney and D. Kilpatrick, Non-Newtonian blood flow in human right coronary arteries: steady state simulations, *J.Biomechanics*, 37 (2004) 709-720.

[3] F. J. H. Gijsen, F. N. van de Vosse and J. D. Janssen, The influence of the non-Newtonian properties of blood on the flow in large arteries: steady flow in a carotid bifurcation model, *J. Biomechanics*, 32 (1999) 601-608.

[4] I. Husain, C. Langdon and J. Schwark, Non-Newtonian pulsatile blood flow in a modeled artery with a stenosis and an aneurysm, *Rec Res Envi Geo Sc*, 413-418.

[5] N. Bernard, D. Coisne, E. Donal and R. Perrault, Experimental study of laminar blood flow through an artery treated by a stent implantation: characterisation of intra-stent WSS, *J.Biomechanics*, 36 (2003) 991-998.

[6] S. Z. Zhao, X. Y. Xu, A. D. Hughes, S. A. Thom, A. V. Stanton, B. Ariff and Q. Long, Blood flow and vessel mechanics in a physiologically realistic model of a human carotid arterial bifurcation, *J.Biomechanics*, 33 (2000) 975-984.

[7] Q. Long, X. Y. Xu, B. Ariff, S. A. Thom, A.D. Hughes and A.V. Stanton, Reconstruction of blood flow patterns in a human carotid bifurcation: a combined CFD and MRI study, *J. Magn Reson Imag*, 11 (2000) 229-311.

[8] J. Chen and X-Y. Lu, Numerical investigation of the non-Newtonian blood flow in a bifurcation model with a non-planar branch, *J. Biomechanics*, 37 (2004) 1899-1911.

[9] J. Chen and X-Y. Lu, Numerical investigation of the non-Newtonian pulsatile blood flow in a bifurcation model with a non-planar branch, *J.Biomechanics*, 39 (2006) 818-832.

[10] E.S. Weydahl and J.E. Moore Jr., Dynamic curvature strongly affects wall shear rates in a coronary artery bifurcation model, *J. Biomechanics*, 34 (2001) 1189-1196.

[11] M. Prosi, K. Perktold, Z. Ding and M.H. Friedman, Influence of curvature dynamics on pulsatile coronary flow in a realistic bifurcation model, *J. Biomechanics*, 37 (2004) 1767-1775.

[12] F. J. H. Gijsen, E. Allanic, F. N. van de Vosse and J. D. Janssen, The influence of the non-Newtonian properties of blood on the flow in large arteries : unsteady flow in a 90^o curved tube, *J. Biomechanics*, 32 (1999) 705-713.

[13] D.Wang and J. Bernsdolf, Lattice Boltzmann simulation of steady non-Newtonian blood flow in a 3D generic stenosis case, *Computers and Mathematics with Applications*, 58(2009) 1030-1034.

[14] A. S. Shuib, P. R. Hoskins, and W. J. Easson, Flow regime characterization in a deseased artery model, *World Academy of Science, Engineering and Technology*, 38 (2010) 100-104.

[15] S. Hyun, C. Kleinstreuer and J.P. Archie Jr, Hemodynamics analyses of arterial expansions with implications to thrombosis and restenosis, *Med Eng Phy*, 22 (2000) 13-27.

[16] M.M. Zarandi, R. Mongrain and O.F. Bertrand, Determination of flow conditions in coronary bifurcation lesions in the context of the Medina classification, *Modelling and Simulation in Engineering*, 2012.

[17] K. Yasuda, R.C. Armstrong and R.E. Cohen, Shear-flow properties of concentrated solutions of linear and branched polystyrenes, *Rheol Acta*, 20 (1981) 163-178.

[18] E. Holzbecher and H. Si, Accuracy tests for COMSOL and Delaunay meshes, *Excerpt from the Proceedings of the COMSOL Conference*, Hannover, Germany (2008).

[19] J. Boyd, J. M. Buick and S. Green, Analysis of the Casson and Carreau-Yasuda non-Newtonian blood models in steady and oscillatory flows using the lattice Boltzmann method, *Phys Fluids*, 19 (2007) 093103.

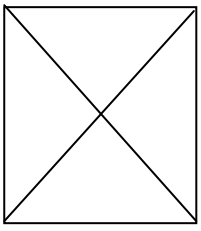

Brief biographies and photos (25 x 30 mm) of authors should be submitted after the paper is accepted. The way of writing the author's biography must follow the style below.

The settings of the font size to prepare the equations are:
Main equation: 9.5 pt (Times New Roman),
Subscript/superscript: 6 pt (Times New Roman),
Sub-subscript: 5 pt (Times New Roman),
Symbol: 18 point,
Sub-symbol: 12 point.